Dynamic heterogeneities versus fixed heterogeneities in earthquake models

Bruce E. Shaw

Lamont–Doherty Earth Observatory, Columbia University, Palisades, NY 10964, USA. E-mail: shaw@ldeo.columbia.edu

SUMMARY

A debate has raged over whether fixed material and geometrical heterogeneities, or alternatively dynamic stress heterogeneities, arising through frictional instabilities dominate earthquake complexity. It may also be that both types of heterogeneities interact and are important. This paper makes a first step in examining this interaction, combining two previously separate lines of research. One line examined friction, which has attractors (the subset of the phase space that the system evolves towards in the long run) on homogeneous faults, which are simple, and then added fixed heterogeneities to the faults to obtain complex attractors. Another line examined frictions, which produced complex attractors on homogeneous faults. Here, we examine frictions, which produce complex attractors on homogeneous faults, and study them on heterogeneous faults, in order to study the interaction of dynamic stress heterogeneities and fixed fault heterogeneities. We consider two types of fixed heterogeneities: an additive noise and a multiplicative noise to the frictional strength of the fault. Because of the linearity of the bulk elastodynamics, the attractor is unaffected by additive fixed noise in the strength of the fault: adding an arbitrary function of space, fixed in time, to the friction leaves the resulting attractor unchanged. In contrast, multiplicative fixed noise multiplying the friction can have a profound effect on the resulting attractor. In the small multiplicative noise amplitude limit, the frictional weakening attractor is little perturbed; at finite amplitudes, fixed heterogeneities substantially alter the attractor. We see, as one consequence, a shift toward longer length events at larger amplitudes. Fixed heterogeneities are seen to reduce the irregularities created by the frictional instability we study, but by no means destroy them. We quantify this by examining a measure of variability of the importance in hazard estimates, the coefficient of variation of large event recurrence times. The coefficient of variation is seen to remain substantial even for large fixed heterogeneities. For friction that weakens with time, so the underlying uniform fault attractor is simple, fixed heterogeneities increase irregularity. For all frictions examined, at low fixed heterogeneity the stress concentrations left over by the ends of the large events dominate where most of the small events occur, while at higher heterogeneity the stress irregularities left over by fixed fault heterogeneities begin to dominate where the small events occur. This may be the strongest signature of fixed heterogeneities, and should be examined further in the Earth. Finally, in what may have important implications for more sophisticated estimates of earthquake hazard, we see a correlation of locations with lower strength drop having higher variation in large event repeat times.

Key words: coefficient of variation, complexity, dynamics, earthquakes, hazard, heterogeneities.

GJI Seismology

1 INTRODUCTION

Earthquakes are complex in many ways. A central unanswered question is why are they complex. Is it because the Earth itself is complex, with a wide variety of material and geometrical heterogeneities seen in fault zones? Or might there be some underlying dynamic reason? In seeking to explain the complexity of the Earth, we seek mod-

els that reproduce the variety of behaviours in the Earth in some statistical sense as they evolve over the long term. An important concept in all of this is an attractor, which is the part of phase space that dissipative systems evolve towards in the long run. Only a part of phase space is visited because with sequences of events, ruptures begin from the conditions left by previous ruptures, and those conditions evolve to be compatible with the dynamics and are not

arbitrary. Attractors can be simple, as simple as a constant or periodic behaviour, and attractors can also be complex, neither periodic nor random, but some structured yet irregular behaviour. Because fault systems evolve little over earthquake cycle timescales and are highly dissipative, following the many previous earthquakes that have occurred earthquake sequences are expected to be evolving along an attractor. The open question is what is the physics that is causing the clearly complex attractor.

A class of frictions that weaken with slip or slip rate has offered the possibility of dynamic complexity even on faults that are completely uniform in their material and geometrical properties. This complexity has shown a wide variety of earthquake behaviours, including the distribution of sizes of events (Shaw & Rice 2000), radiated energy–moment scaling relations (Shaw 1998), and magnitude dependent radiated energy spectra (Shaw 2003). This complexity has been shown to persist across a range of dimensions, including 1-D (Carlson & Langer 1989), 2-D (Cochard & Madariaga 1996; Myers *et al.* 1996; Shaw 1997) and 3-D scalar models (Shaw & Scholz 2001), and a variety of dispersive bulks, including the wave equation (Shaw 1997) and the Klein–Gordon (Myers *et al.* 1996) equations. One measurement in three dimensions has suggested that the dynamic complexity may be an essential part of earthquake behaviour: slip-length scaling relations for large earthquakes were reproduced with a uniform 3-D model, not only in the mean, but in the variance as well (Shaw & Scholz 2001). This suggested that dynamic heterogeneities were already of the order of the variance observed in at least one measure of earthquake behaviour. Are dynamic heterogeneities dominant? Are static fixed heterogeneities dominant? Might some mixture of both types of heterogeneities be relevant? By dynamic heterogeneities, we mean evolving heterogeneities, such as slip and stress heterogeneities, which change during earthquake events. By fixed heterogeneities, we mean heterogeneities, which do not evolve in time, or perhaps evolve only very slowly over geological timescales (also called 'quenched' heterogeneities in the physics literature).

While many researchers have suggested that fixed heterogeneities must be dominating earthquake behaviour, they have often been driven to this conclusion by a lack of complexity without fixed heterogeneities, due to the intrinsic simplicity of the underlying dynamic attractor for the frictions considered (Xu & Knopoff 1994; Ben-Zion & Rice 1995; Wang & Hwang 2001). Other papers have also examined the dynamic modelling of earthquakes with fixed heterogeneities (Knopoff *et al.* 1992; Lin & Taylor 1994; Nielsen *et al.* 1995; Fisher *et al.* 1997). Nevertheless, the full spectrum of complex behaviours displayed by earthquakes has yet to be explained by any model. Here, we explore this question from a very different point of view. We begin from frictions that produce an underlying dynamically complex attractor. Then, by perturbing away from the uniform case with fixed heterogeneities, we ask how the attractor is altered.

The remainder of the paper is organized as follows: in the next section, Section 2, we discuss the basic model, and the perturbations to the friction. In Section 3, we present results with fixed heterogeneities. Finally, in Section 4, we discuss the generality of the results, and then conclude.

2 THE MODEL

The basic 2-D model we use has been presented before (Shaw 1997; Shaw & Rice 2000). The one new feature that we add is a generalization of the friction to consider spatial heterogeneities. Readers familiar with the model may skip this Section 2, noting the gener-

alization of the friction presented below in eq. (6), and proceed to Section 3.

We consider here the case of the planar fault. This has the advantage of being vastly easier to solve numerically. As we will see, it also preserves a symmetry, which allows a remarkable invariance of the system. At the end we will discuss the implications of our planar results for the non-planar case.

We make a couple of other simplifications as well, none of which will be important to our calculations. First, we look at a lower-dimensional model. This offers a tremendous speedup numerically, allowing for a much expanded exploration of parameter space. We focus here on a 2-D model, where the loading from the deep stably sliding fault occurs a crust depth away from the seismogenic fault. A second simplification is we consider numerically the antiplane case, so that there is only a single scalar mode, and we have the wave equation in the bulk. In our discussions surrounding the results, we will generalize to the tensor case, but it is simplest here to focus on the scalar case. Fig. 1 illustrates the geometry of the model.

The equations of motion are then as follows. In the bulk we have the wave equation for the displacement U:

$$\frac{\partial^2 U}{\partial t^2} = \nabla^2 U, \tag{1}$$

where t is time, and $\nabla^2 = \partial^2/\partial x^2 + \partial^2/\partial y^2$ is the 2-D Laplace operator. We take x to be the direction parallel to the fault and y the direction perpendicular to the fault. We use dimensionless units throughout, to minimize the number of parameters. Here we have set the speed of sound to unity. On the fault, located at $y = 0$, we have a frictional boundary condition, which relates the strain to the tractions T,

$$\left. \frac{\partial U}{\partial y} \right|_{y=0} = T. \tag{2}$$

The tractions consist of two parts,

$$T = \Phi - \eta \nabla_\parallel^2 \frac{\partial S}{\partial t}. \tag{3}$$

The first part, the friction Φ, contains all the non-linearity, and is central to the problem. We will return to discuss this shortly. The second part is a viscous-like term added to provide stability at the small scales. The parameter η is the strength of this boundary dissipation, $\nabla_\parallel^2 = \partial^2/\partial x^2$ is a fault-parallel Laplace operator and $\partial S/\partial t = \partial U/\partial t|_{y=0}$ is the slip rate on the fault. This term is useful for providing a good continuum limit, but is not otherwise qualitatively important in the resulting behaviour (Langer & Nakanishi 1993; Shaw 1997; Shaw & Rice 2000). Here we separate it from the main friction term since it allows for a simpler treatment when we consider multiplicative perturbations.

Along the direction of the fault we use periodic boundary conditions to maintain the translational symmetry in the uniform fault case:

$$U(x + L_x) = U(x). \tag{4}$$

Away from the fault, the boundary is slowly loaded:

$$\left. \frac{\partial U}{\partial t} \right|_{y=1} = \nu, \tag{5}$$

where $\nu \ll 1$ is the slow plate loading rate. We have scaled distances in the problem by the distance to the loading surface, so that it is located at $y = 1$. This scaling corresponds to setting the seismogenically active depth, a length-scale of order 15 km in strike-slip environments, to unity.
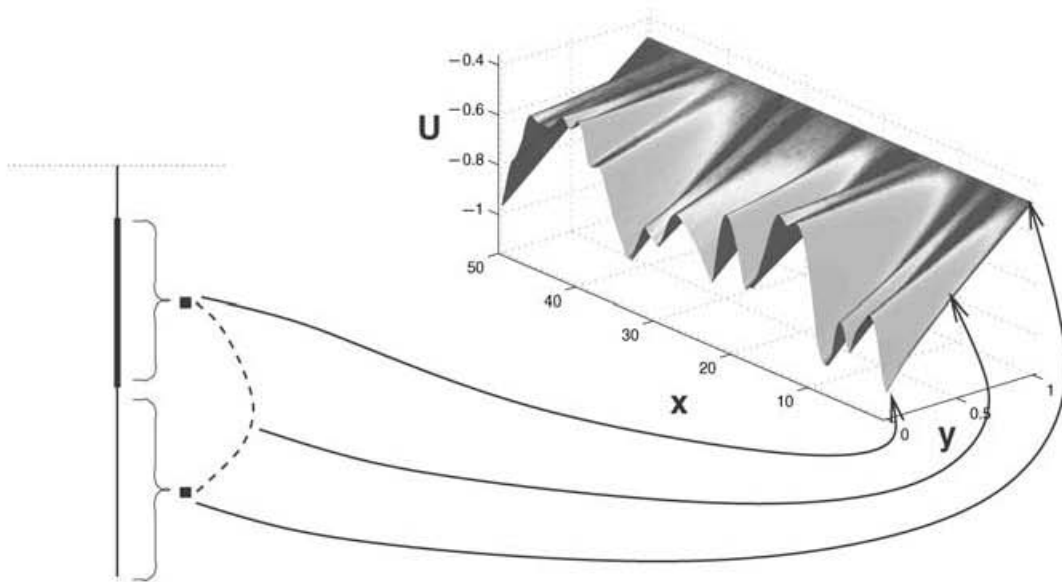
Figure 1. Illustration of the geometry of the model. The schematic on the left is a cross-section with depth of a vertical strike-slip fault. At the top is a free surface, indicated with a dotted line. The seismogenic fault is indicated with a thick solid vertical line, and the stable sliding shallow fault and deep fault are indicated with thin solid lines. The planar fault continues along the strike back into and out of the plane of the page. We collapse this geometry on to a lower dimension by collapsing the seismogenic fault depth to a point and the stable sliding fault depth to a point, and collapse the connecting elastic interaction between them to a line, indicated by the dashed line connecting the seismogenic point and the stable sliding point. The brackets portray the collapse of the depth direction to points. As before, the direction into and out of the page contains the fault along strike. A perspective view of this 2-D model that includes the along-strike direction is shown on the right, with the vertical axis plotting displacement. Lines capped by arrows shown how the collapsed cross-section on the left maps on to the corresponding parts of the perspective view on the right, with the dashed line mapping on to the interior, and the seismogenic fault and stable sliding fault mapping on to the boundaries. The perspective view on the right shows a snapshot of the model at a point in time when the fault is stuck, and also indicates the irregular nature of the attractor, with the non-constant displacement that has evolved along the seismogenic fault boundary.

The key to the problem is the friction. All of the non-linearity in the problem is there. Previous work has shown that a richly complex attractor can arise in the case where the friction is a uniform function along the fault. In this paper, we generalize the friction to consider two types of perturbations, which are functions of space, but fixed in time. One will be an additive function, and the other multiplicative. Thus, we generalize to:

$$\Phi \rightarrow a(x) + [1 + n(x)]\Phi \qquad (6)$$

so that when $a(x)$, the additive fixed term, and $n(x)$, the multiplicative fixed term, both vanish, we are left with the unperturbed uniform case. a and n will be real functions of space, fixed in time. Friction is equal to the normal stress multiplied by the coefficient of friction. Hence we use n in the notation of the multiplicative term to connect to the way that normal stress variations would enter. Adding a constant strength to the fault would map into the a term.

When Φ weakens with slip or slip rate, a remarkably rich attractor can arise. The form of Φ we consider here has been examined extensively (Shaw 1997; Shaw & Rice 2000). The physical motivation goes back to Sibson (Sibson 1973), wherein frictional sliding generates heat, thereby raising the pore fluid temperature and pressure and, thus, decreasing the effective normal stress and friction. This gives frictional weakening from frictional heating. Our constitutive equations make a simple mathematical quantification and approximation of this effect. In addition to the physical motivation, they also have the advantage of spanning a range of frictional instabilities, from slip weakening in one limit to velocity-weakening in another. This friction has been described previously, and those familiar with it and those unconcerned with the details are invited to skip the next friction section.

2.1 The friction

Using an approximation (Shaw 1997) of the full non-linear case (Shaw 1995), our constitutive equations for the friction Φ are

$$\Phi = \phi\left(\frac{\partial S}{\partial t'}, t' \leq t\right) H\left(\frac{\partial S}{\partial t}\right). \qquad (7)$$

Here $\partial S/\partial t = \partial U/\partial t|_{y=0}$ is the slip rate on the fault, with ϕ depending on the past history of slip. The function H is the antisymmetric step function, with

$$H = \begin{cases} \widehat{\dfrac{\partial S}{\partial t}} & \dfrac{\partial S}{\partial t} \neq 0; \\[2mm] |H| < 1 & \dfrac{\partial S}{\partial t} = 0, \end{cases} \qquad (8)$$

where $\widehat{\partial S}/\partial t$ is the unit vector in the sliding direction. Thus H represents the stick-slip nature of the friction, being multivalued at zero slip rate: it takes on whatever value is needed to resist motion up to some threshold in the stick phase and resists against the direction of motion above that threshold in the slip phase. H maps a positive scalar strength ϕ into a traction having a direction Φ.

The history-dependent ϕ we examine in this paper is given by

$$\phi = \Phi_0 - \frac{\alpha Q}{1 + \alpha Q} - \Sigma \qquad (9)$$

with

$$\frac{\partial Q}{\partial t} = -\gamma Q + \left|\frac{\partial S}{\partial t}\right|. \qquad (10)$$

Here Φ_0 sets the threshold value of sticking friction, which as long as it is large compared with the maximum friction drop, turns out to be

an irrelevant parameter in the problem. The variable Q is something like heat; it accumulates with increasing slip rate on the fault and dissipates on a timescale $1/\gamma$. An equivalent integral solution of Q

$$Q(t) = \int_{-\infty}^{t} e^{-\gamma(t-t')} \left| \frac{\partial S}{\partial t'} \right| dt' \qquad (11)$$

shows that when $1/\gamma$ is large compared with the rupture timescale of unity, Q is just the slip, while when $1/\gamma$ is small, Q rapidly reaches a steady state value of $1/\gamma$ times the slip rate. Thus γ controls the relative amount of slip-weakening versus velocity-weakening effects (Shaw 1995).

The parameter α is the rate of weakening at small Q, which turns out to be a crucial parameter. It has dimensions of inverse length. The denominator $1 + \alpha Q$ is used so as to saturate the drop in friction caused by this term at large Q, with the strength drop scaled to unity.

The third term in the friction, Σ, describes the stress drop in going from sticking to sliding friction. We make a gross simplification of this term and, for simplicity, consider a Σ that weakens with time, giving a time-dependent nucleation

$$\Sigma = \begin{cases} \sigma_0 \dfrac{t - t_s}{t_0} & t - t_s < t_0; \\ \sigma_0 & t - t_s \geq t_0 \end{cases} \qquad (12)$$

so that Σ increases linearly with time once the fault becomes unstuck, up to a maximum value σ_0 over a timescale t_0, and is reset to zero when the fault resticks. The time t_s is measured from the last unsticking and is reset during an event if the fault resticks and then slips again. Other nucleation mechanisms such as slip weakening give similar behaviour for properties such as the distribution of sizes of events (Shaw & Rice 2000). This time-dependent nucleation has the advantage that it allows for a complete separation of timescales between the loading and rupture timescale, greatly speeding up the numerics. The specifics of Σ are unimportant to the results we present in this paper.

This Σ term is a substantial simplification of what is likely to be happening in the Earth. A more realistic representation of this term would be the rate-and-state formulation (Dieterich 1979; Ruina 1983); but that formulation is much more expensive numerically, and it has been shown that many of the features of the model are insensitive to the details of the Σ term, at least in the 2-D models (Shaw & Rice 2000).

2.2 Numerics

We numerically solve the model equations with a finite-difference second-order explicit scheme. We solve with grid resolutions δ_x and δ_y, a fraction of the seismogenic depth (which is scaled to unity) and the time steps, a fraction of the grid spacing. The time-dependent nucleation we use has the advantage that we can separate the loading and rupture timescales, taking the limit of zero loading speed, simply load the system between events to their threshold, and then take $v = 0$ during an event. At the end of an event, we quench the dynamic waves to the static elastic solution; we then reload the system until the next part of the fault is just at the threshold for failure. Further discussion of the numerics can be found in Shaw & Rice (2000).

In the numerical simulations, we choose the following as a canonical set of parameters, about which we vary. The qualitative aspects of the results we discuss do not appear to be sensitive to any of these parameters. For the bulk, the fault length $L_x = 200$, the grid resolutions $\delta_x = 1/10$, $\delta_y = 1/20$. For the traction, $\eta = 0.003$, $\sigma_0 = 0.03$, $t_0 = 0.2$, $\alpha = 3$ and $\gamma = 0.1$, giving slip-weakening.

Fig. 2 illustrates the complex attractor that arises in this model in the uniform friction case when $a(x) = n(x) = 0$.

Fig. 3 shows the distribution of sizes for various values of α.

3 RESULTS FOR FIXED HETEROGENEITIES

3.1 Additive noise

We find that there is an elegant symmetry in the planar fault problem, which makes the attractor invariant with respect to additive noise. That is, we can add an arbitrary change in strength along the fault,
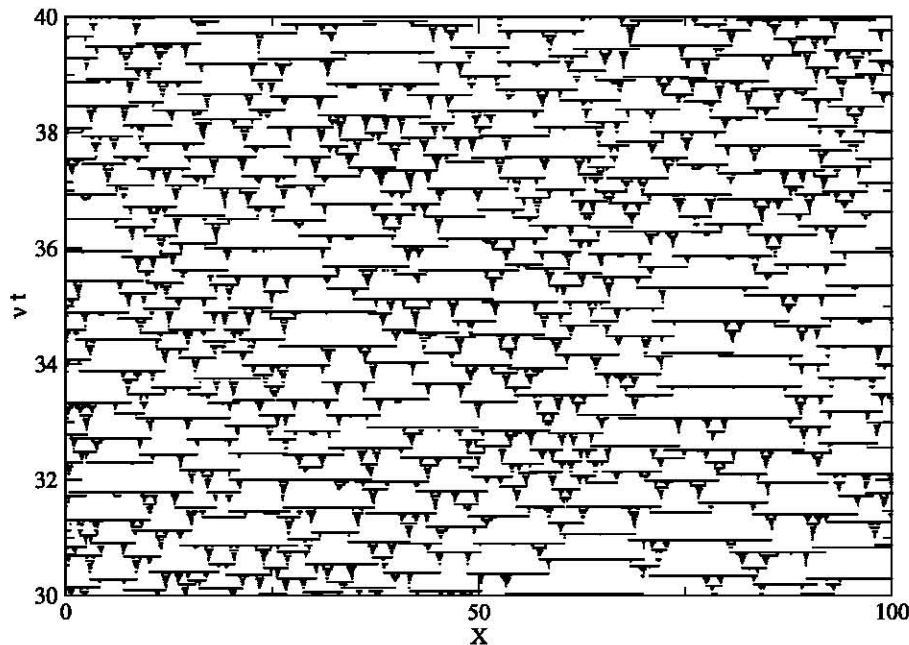

Figure 2. A projection of the complex attractor in the uniform fault case, showing the time at which events along the fault slipped.
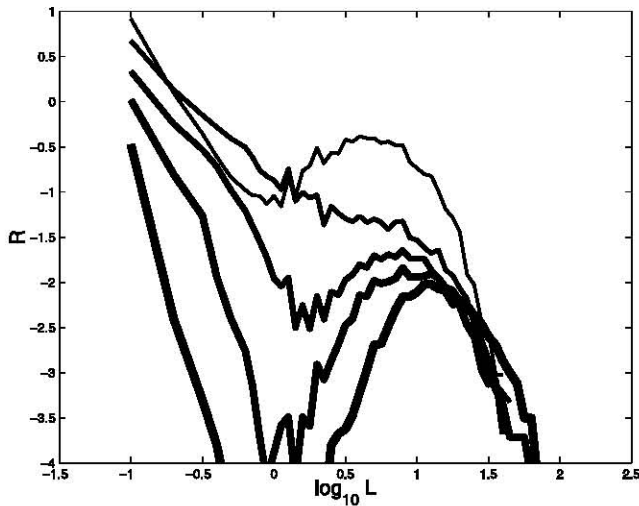
Figure 3. Distribution of lengths for uniform fault case. The different curves are for different frictional weakening α values. Increasing line thickness corresponds to increasing weakening, with $\alpha = 1, 2, 4, 8$ and 12, respectively.
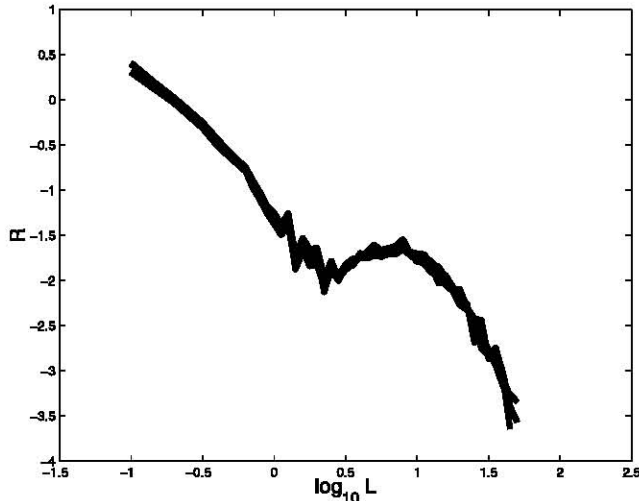

Figure 4. Distribution of lengths for additive noise case. $A = 0, 1, 10$ and 30. Note overlaying of curves.

and in the long run the behaviour along the fault will be the same. Fig. 4 illustrates this invariance where we plot the distribution of sizes of events for the case of additive random white noise with a wide range of amplitudes:

$$a(x) = A\xi(x) \tag{13}$$

with $A = 0, 1, 10, 30$ and ξ being uncorrelated white noise:

$$\xi \in [0, 1],$$
$$\langle \xi(x)\xi(x')\rangle - \langle \xi(x)\rangle^2 = \tfrac{1}{12}\delta(x - x'). \tag{14}$$

Despite variations in the strength as much as 30 times larger than the strength drops, all the curves overlay.

In retrospect, this is understandable, since it is only strength drops, and not absolute strength, which matter in the dynamics. An obvious symmetry in the problem

$$\Phi \to \Phi + \lambda \qquad U \to U + \lambda y \tag{15}$$

shows that we can add a constant strength and counteract it with a constant strain and leave the equations of motion invariant. What is less obvious, but nevertheless true, is that we can add an arbitrary function of space to the fault and still have it scale out. The boundary integral representation relation for linear elasticity tells us that we can write the stress perturbations of faults caused by displacement discontinuities on faults, and vice versa the displacement discontinuities, which reproduce stress perturbations on faults, with integrals over faults:

$$S(x, t) = \int_{-\infty}^{t}\int_{\Gamma} G(x', x; t', t)\tau(x', t')\,dx'dt', \tag{16}$$

where S is the slip perturbation and τ is the traction perturbation on the fault Γ. On planar faults, the Green functions G for 2-D have been solved by Lamb (1904) and in 3-D by Richards (1979). At long times when everything is at rest, this tells us that adding a specific choice of slip on the fault could exactly cancel a fixed spatially varying stress on the fault. Combined with the representation theorem for elasticity, relating displacements on the fault to displacements in the bulk, we see that there is a generalization of eq. (15) that allows for the exact cancellation of not only a constant λ, but a spatially varying $\lambda \to a(x)$. It is a test of the numerics that it indeed picks up this symmetry of the equations, as Fig. 4 illustrates.

3.2 Multiplicative noise

The case of multiplicative noise is substantially different from that of additive noise. Here, we can dramatically alter the attractor. It does not, however, appear to be a singular perturbation; the complex dynamic attractors in the uniform case appear to be structurally stable to small multiplicative fixed perturbations. That is, small perturbations only make small changes in the attractor. Fig. 5 shows the distribution of sizes for white noise $n(x) = \mathcal{N}\xi(x)$ with amplitudes $\mathcal{N} = 0, 0.1, 0.5, 1, 2$ and 4. Note the overlap of the unperturbed and very small perturbation case, and then the progressive
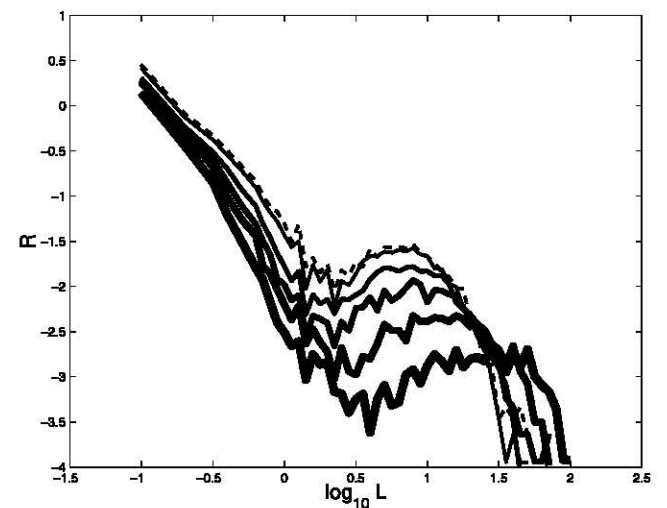

Figure 5. Distribution of lengths for multiplicative noise case. The uniform fault case $N = 0$ is shown with a dashed line, and then the multiplicative noise cases are shown with solid lines of increasing thickness for increasing amplitude, $N = 0.1, 0.5, 1, 2$ and 4. Note the overlaying of the unperturbed case and the smallest noise case.
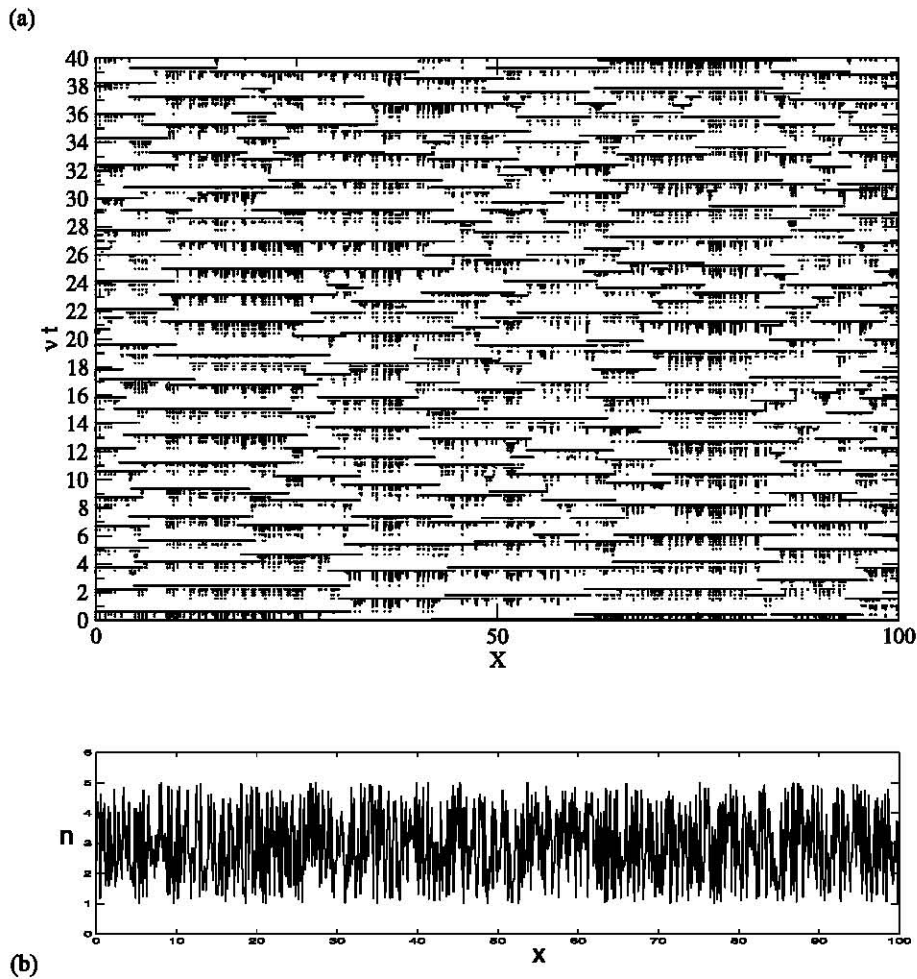
(a)

(b)

Figure 6. (a) Representation of the complex attractor for the multiplicative noise case, showing the time at which events along the fault slipped. The noise amplitude is $N = 4$. (b) The fixed multiplicative function $n(x)$ for this case.

difference for larger amplitudes. Note also, in comparison with Fig. 3, how at higher amplitudes the largest events are getting longer. This lengthening of the largest events is not just an effect of the rescaling of α, which, among other things, the n term does. The lengths are in fact longer even than the distribution of lengths are if we take $n(x) = \mathcal{N}$, rather than $n(x) = \mathcal{N}\xi(x)$, so n has the constant upper value compared with the random amplitude case. Thus, the fluctuations are playing a fundamental role in altering the distribution of static and dynamic stresses, which contribute to the distribution of lengths of events.

Finite values also start to show quantitative differences from the uniform case with the breaking of translational invariance. Thus some points on the fault consistently slip much more during large events, and some slip much less; since they have to all slip the same amount in the long run, smaller events then occur at the parts that slipped less to make up the difference. These patterns of where the small events are occurring become tied, or pinned, to the locations along the fault in this heterogeneous fault case, in contrast to the homogeneous fault case, illustrated in Fig. 2, where in the long run all points along the fault behave the same. This is easiest to visualize by projecting, as in Fig. 2, on to the time at which different parts of the fault break. Fig. 6 illustrates this, along with the irregular $n(x)$ multiplying the friction, below.

3.3 Spatial anisotropy

We can quantify the pinning in the problem with a measure of the breakdown of isotropy. The normalized spatial variance measure

$$\Delta \equiv \left\langle \left(\frac{\langle\Theta\rangle_t}{\langle\Theta\rangle_{x,t}} - 1 \right)^2 \right\rangle_x^{\frac{1}{2}} \tag{17}$$

quantifies the degree of isotropy. Here the subscripts x and t on the brackets denote averaging of the variable, Θ, over the space dimension x and time dimension t, respectively. When all points in space are equivalent, the time average at a point $\langle \ \rangle_t$ equals the time average averaged over all space $\langle \ \rangle_{x,t}$ and thus $\Delta = 0$. As points in space become less alike, Δ will increase.

For the variable Θ, the conservation law that, in the long run, all points keep up with the plate loading rate v means that both the average amount of slip per event, and the average time interval between events will both give the same answer. Thus we use this class of equivalent variables for Θ; we measure Θ by measuring the number of events over some time interval, which thus gives the average time interval and also, for a long enough sequence, the average slip.

We can use this spatial variance measure Δ to examine the break-down of isotropy as we increase the multiplicative noise amplitude
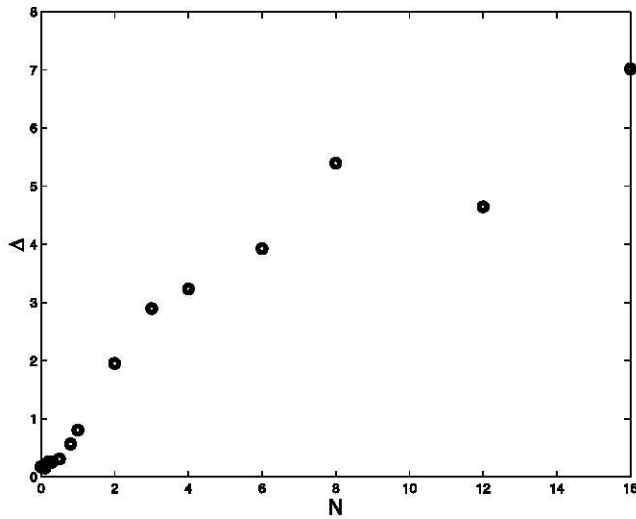
Figure 7. Spatial variance in repeat times as a function of multiplicative noise amplitude $\mathcal{N}$. The scatter in the data is due to the finite lengths of the catalogue.

Figure 8. Coefficient of variation for varying α. The fault is uniform, with $n = 0$. The (+) symbols are for C'_T, while the (o) symbols are for C^*_T.

$\mathcal{N}$. Fig. 7 shows this result. Note the very small values of Δ for small $\mathcal{N}$, with the increase beginning when $\mathcal{N} \sim 1$, where the stress drop perturbations become of order the unperturbed stress drops. The scatter in the data is due to the finite lengths of the catalogue.

3.4 Coefficient of variation

One of the most important parameters in earthquake hazard estimates is, along with the mean recurrence time interval between large events, the coefficient of variation of the recurrence time. The coefficient of variation is given by the standard deviation of the recurrence time divided by the mean recurrence time:

$$C_T \equiv \frac{\sqrt{\langle T^2 \rangle - \langle T \rangle^2}}{\langle T \rangle}. \tag{18}$$

This parameter expresses the relative irregularity of repeat times, with a coefficient of zero implying constant repeat intervals and a coefficient of unity occurring for a random exponential distribution of repeat times. Typical values used in hazard estimates are around 0.2–0.4 (Nishenko & Buland 1987; Ellsworth *et al.* 1999; Lindh 2003), though there is much debate as to what the appropriate values are, with important implications for earthquake hazard and predictability in the balance (Lindh 2003). Here, we use this important parameter to quantify the irregularity of large event repeat times.

To obtain a baseline for the uniform fault case, Fig. 8 shows the variation in C_T for $n = 0$ and different values of α. To calculate C_T we keep track at each point along the fault of all the times when that point on the fault slipped greater than some minimum amount δ_c. We then calculate the average and variance, and then the coefficient of variation at each point on the fault, and finally, to obtain a coefficient of variation for the whole fault, average the coefficients of variation over all the points on the fault. In Fig. 8 we set the minimum slip cut-off values δ_c in two different ways. In the upper set of points, we fix δ_c to be a fixed constant value for all the α values, with $\delta_c = 0.05$ used here for the (+) symbols. (We denote the C_T for this fixed δ_c procedure as C'_T in what follows.) This value of δ_c excludes the small events, and is similar to what we would do with a palaeoseismic trench; since the peak slip of the large
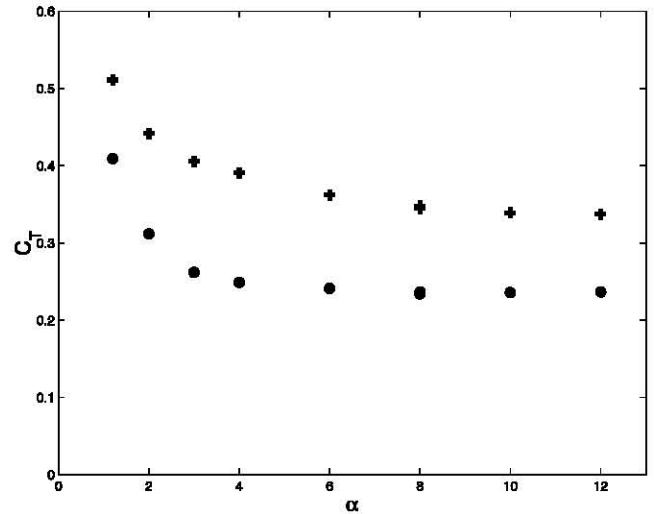
events is around unity, this would correspond to a cut-off of tens of centimetres of slip for typical large events slipping many meters. In the lower set of points, shown with the (o) symbols, we use a minimization process, which finds, for the whole fault, the value of δ_c that minimizes the C_T for the fault. (We denote the C_T for this minimized δ_c procedure as C^*_T in what follows.) This minimized δ_c is typically a substantial fraction of the mean slip of large events, and thus excludes some parts of the rupture we would clearly identify as having ruptured, and also excluded some moderately large events altogether. It does, however, give a lower bound to C_T. It also rules out the possibility that effects we see in C_T variability with changing α and later $\mathcal{N}$ are due to simple changes in the overall scale of the slip events. Comparing the two sets of symbols in Fig. 8, we see they both tell a similar story: we see higher values at smaller α, and what appears to be an approach towards saturation at large α (we are limited in how high a value of α we can resolve numerically, Shaw & Rice 2000). The main difference between the two sets is simply an overall lowering of C_T for the case where it is minimized.

What happens when we add fixed heterogeneities? Fig. 9 shows the mean C_T over the fault for fixed $\alpha = 3$ and increasing values of $\mathcal{N}$. Note the decrease with increasing $\mathcal{N}$, and again what appears to be an approach towards saturation at the highest values of $\mathcal{N}$. This is qualitatively similar to what we saw with increasing α in Fig. 8, and increasing $\mathcal{N}$ tends to increase the effective α since it multiplies it. However, quantitatively we note that the minimum value of C^*_T reached for larger $\mathcal{N}$ is significantly below the C'_T reached for larger α, and thus the fixed heterogeneities are reducing the temporal irregularity. However, note that the C_T remains finite: the irregularity appears to not be going away.

Another slice in parameter space shows similar features; in Fig. 10 we fix $\mathcal{N} = 4$ and vary α. Again there is a decrease with increasing α, and what appears to be an approach towards saturation. And again we see smaller values of C_T compared with the $\mathcal{N} = 0$ case. Thus there is nothing special about the $\alpha = 3$ case of Fig. 9, and typically we are seeing the heterogeneities reducing C_T.

We can learn something by considering not only the average over the fault, but looking at the disaggregate and examining the spatial dependence of this temporal variability. The lower panel of Fig. 11, Fig. 11(b), shows a superposition of three plots; two are the local
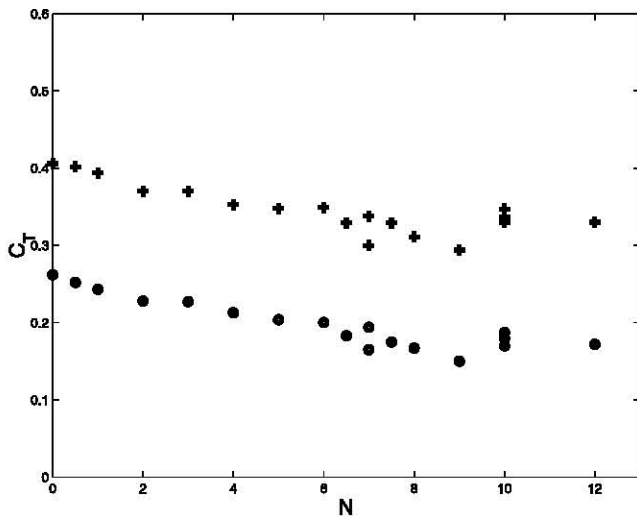
Figure 9. Coefficient of variation for fixed $\alpha = 3$ and increasing amplitude N. The different points are for different runs and the scatter indicates the variations in the data from different spatial heterogeneities.
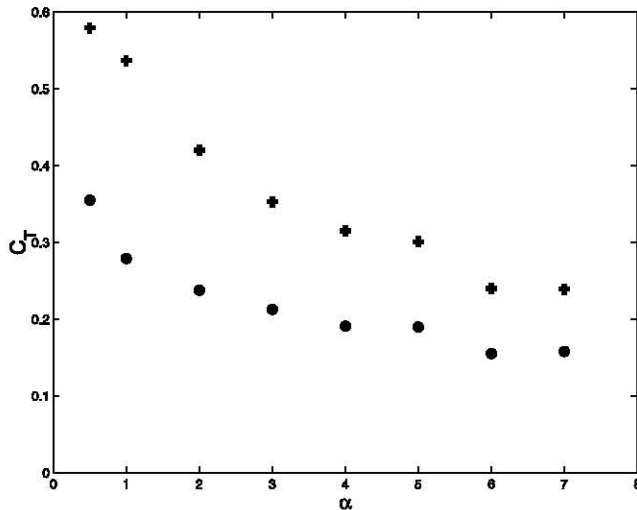

Figure 10. Coefficient of variation for fixed $N = 4$ and increasing α.

coefficients of variation $C_T^*(x)$ and $C_T'(x)$, and the third is a linear transformation of the multiplicative noise $n(x)$. We linearly transform $n(x)$ by multiplying it by a small negative number and adding a constant to it. We do this to show more clearly its correlation with C_T (actually, anticorrelation, hence the negative number; we plot $bn + m$ with $b = -0.1$). We see the C_T being forced by but low pass filtering in some way the $n(x)$. We see $n(x)$ correlating with both measures of C_T, though even more strongly with C_T' than with C_T^*. Fig. 11(a), shows as before in Fig. 6 the times at which various parts of the fault broke, only here in higher resolution along the fault so as to show the spatial correlation with $C_T(x)$ and $n(x)$ in Fig. 11(b). A comparison shows the population of persistent small events, traced by the points vertically aligned in Fig. 11(a), located where the peaks of $-n(x)$ are (the minima of $n(x)$), and correlating well with the peaks of $C_T'(x)$. It is worth emphasizing these interesting results: the low strength drop locations both engender more small events and also have more irregular repeat times for large events.

4 DISCUSSION

Having examined the interaction of dynamic heterogeneities with fixed heterogeneities in our scalar planar 2-D model with one class of friction laws, an immediate question is how do these results generalize? Let us first consider the various model simplifications we do not expect to matter. Regarding the role of dimensionality, this appears to be unimportant to the results. We have recovered the same results using a 1-D model (where the continuous degree of freedom perpendicular to the fault y is collapsed to the fault, making the model geometry more like a rubber band than a rubber sheet (Carlson *et al.* 1994)). We have also explored the scalar 3-D generalization with an unstable sliding fault layer, a stable sliding lower fault, and a free surface at the top (Shaw & Scholz 2001). Here again we see the same qualitative results reported here (although because of the computational expense we are of course unable to explore parameter space as fully). Thus, again, the dimensionality of the model appears to be unimportant. With regard to the role of the scalar approximation, for planar faults this should again be unimportant, since motions along the fault only affect shear stresses and not normal stresses, in the absence of material contrasts (Weertman 1980; Andrews & Ben-Zion 1997) or dipping faults near a free surface (Brune 1996; Oglesby *et al.* 1998).

Other aspects of the simplified model are similarly unimportant. For example, the details of the loading geometry, represented here by a stiff boundary a fault depth $y = 1$ away, do not matter. Alternative 2-D geometries such as loading on the bottom, giving a dispersive bulk Klein–Gordon equation (Myers *et al.* 1996) or loading on the fault combined with radiating transparent boundaries away from the fault (Shaw 2003) give similar behaviours.

Regarding the parameter space of the model, while we chose as our canonical set of parameters to perturb about the values where the attractor in the uniform fault has not only large event complexity but small event complexity as well, our basic results are not restricted to any small parameter range. To begin with, large event complexity is the typical—not exceptional—result. Furthermore, the parameter space where numerous small events occur is expanded by the fixed perturbations, not diminished.

Let us turn now to simplifications that do have more of an impact. The linearity of the bulk allowed the possibility of a sweeping invariance to absolute strength, and thus the invariance to additive noise and the statement that only strength drops, not strength mattered. This invariance can be broken through a variety of mechanisms, and thus will less typically hold in more general situations. Some mechanisms that break the invariance are a non-linear bulk (a situation rarely if ever considered by modellers, but one that may be relevant in the real case, particularly close to the fault), non-planar faults (in which case strength changes couple to normal stress variations and thus couple through the friction in a multiplicative way) and frictional formulations tied more directly to the absolute strength. Thus, for example, in this latter case of frictional formulations, a fuller accounting of heating effects would have a strength effect in the heat generating term in the friction (the last term in eq. 10, Shaw 1995), corresponding to a multiplicative perturbation of the weakening parameter α. Our examination of the multiplicative noise case can thus subsume many of the anticipated additive noise effects under more general conditions. The additive noise invariance in our simple model is a convenience for exploring parameter space, and helps to indicate a more general point— that it is fundamentally strength changes that matter in the dynamics (note that in the latter two examples above where the additive
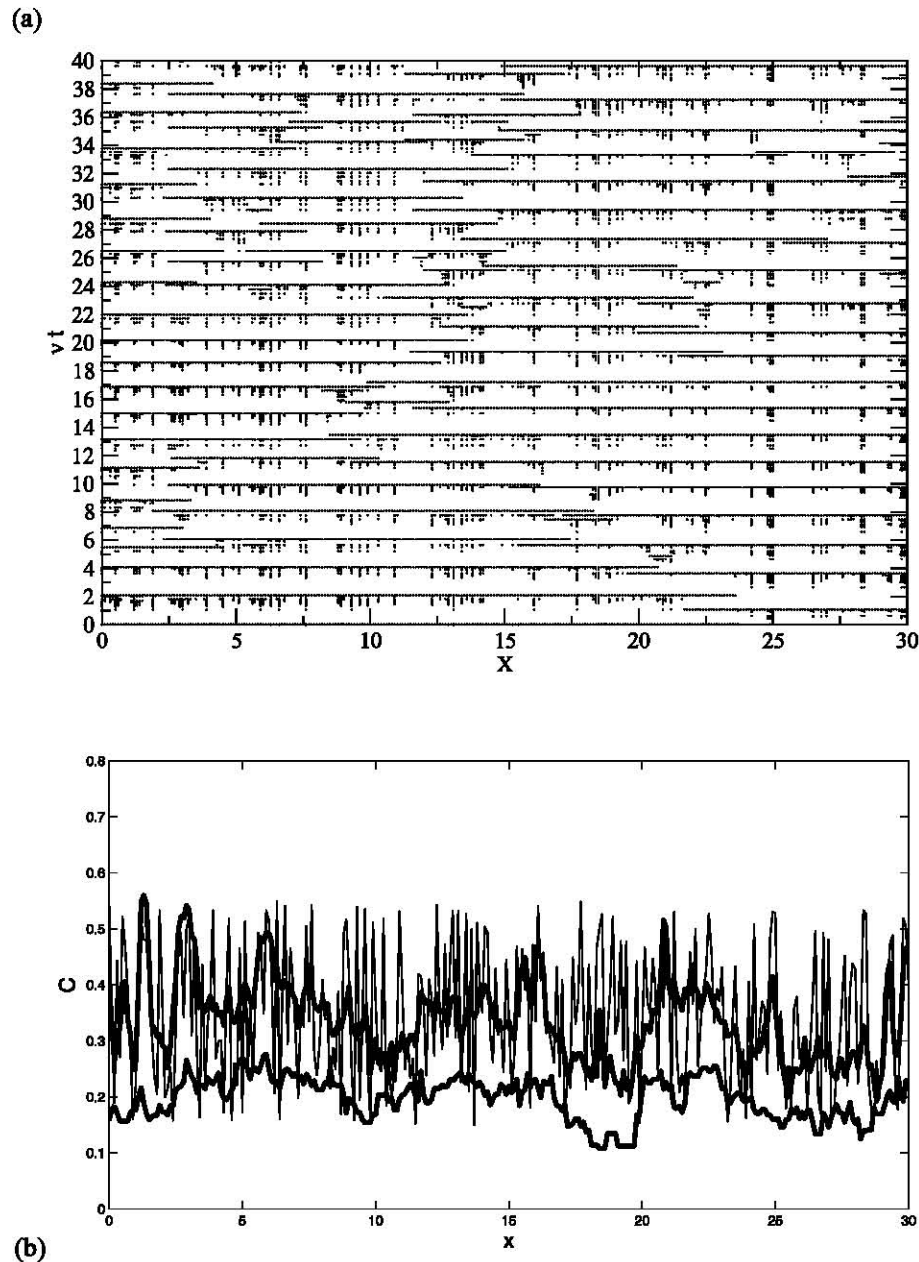
(a)

(b)

Figure 11. (a) Representation of the complex attractor for the multiplicative noise case, showing the time at which events along the fault slipped. As in Fig. 2, the noise amplitude is $N = 4$ and the slip weakening parameter $\alpha = 3$. (b) The coefficient of variation C'_T and C^*_T, plotted in the upper and lower thick lines, respectively, and a linear transformation of the multiplicative noise $n(x)$, plotted with a thin solid line. The linear transformation shown is $-0.1 \times n(x) + 0.65$. Note the anticorrelation of C_T and n, demonstrated by the lining up of the peaks of the lines. Note also the lining up of the location of small events in (a) with the peaks of the thin solid line, the minima of $n(x)$.

invariance was lost, it was through its feedback on to the strength changes).

Relaxing the assumption of planarity of the fault opens up potentially significant changes. Dynamic normal stresses now result not only in multiplicative changes of the strength, but *dynamic multiplicative* changes. This opens up a whole new realm of potential feedbacks that our constant multiplicative exploration cannot fully cover here. This therefore remains the most significant question, and deserves top priority for future research. Non-planar models for individual ruptures have been successfully simulated by a number of groups. To address the questions we have posed in this work, however, long sequences of ruptures will need to be simu-

lated on non-planar geometries, a regime yet to be reached in the literature.

Finally, we have focused our attention here on one class of frictions, those that weaken initially linearly with slip or velocity, and some mixture of the two. What about other frictions beyond this class? Probably the most important aspect of our frictions are that they already produce complexity even in the uniform fault cases, generically for the large events and in a relatively narrow parameter range for the small events (Shaw & Rice 2000). A friction that did not produce a complex attractor, such as a time weakening friction (Nielsen *et al.* 1995) or rate and state friction with a single slip weakening length (Ben-Zion & Rice 1995) could obviously not have an
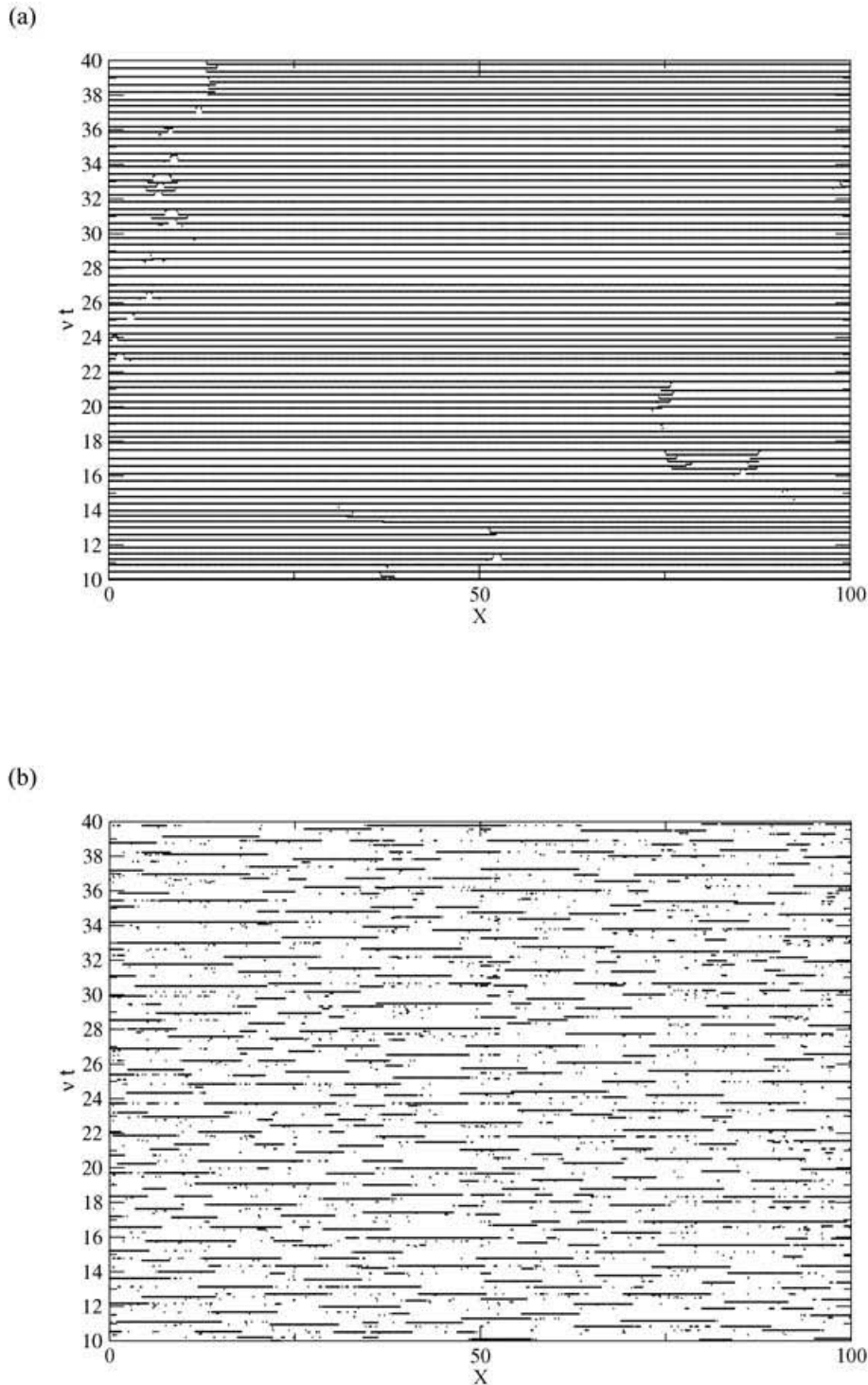
(a)

(b)

Figure 12. (a) Representations of the attractor for the time weakening friction case. (a) No noise $N = 0$ shows a simple attractor. (b) $N = 4$ gives a complex attractor.

attractor made any simpler by fixed noise. Examining a time weakening friction (with small velocity strengthening), $\alpha = 0$ and $\sigma_r > 0$, we see a quite different effect of heterogeneities: here, increasing heterogeneities increase the variability from the simple uniform fault case. Fig. 12 shows two example attractors, a simple one when $N = 0$ and a complex one when $N = 4$. Fig. 13 shows the coefficient of variation for increasing N. Note again the apparent approach

to an asymptotic value at large N. Note also, interestingly, that the asymptotic heterogeneity is actually higher than in the $\alpha > 0$ case (In fact, the asymptotic value appears to decrease with increasing α.) These two different kinds of behaviours, a complex unperturbed attractor made more regular by heterogeneities, and a simple unperturbed attractor made more irregular by heterogeneities, show the richness of potential interactions.
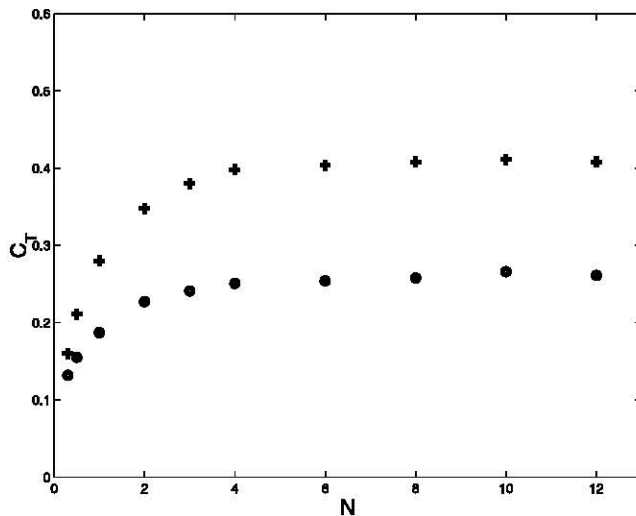
Figure 13. Coefficient of variation for time weakening $\alpha = 0$ and increasing N. Note that now the irregularity is increasing with increasing noise. Note also that the irregularity appears to saturate for large N.

In both cases, however, we see a commonality arising when viewed spatially. At low heterogeneity, the stress concentrations left over the ends of the large events dominate where most of the future small events occur (Shaw 2000). At larger heterogeneity, the stress irregularities left over by fixed spatial friction irregularities begin to dominate where most of the small events occur. This, then, may be the strongest signature of fixed heterogeneities.

4.1 Conclusions

Seismologists often talk about the strength of faults. However, as this work reaffirms, it is fundamentally strength drops, not the strengths themselves, which are the quantity relevant to earthquake behaviour. To the extent that absolute strength can feed back on to strength drops, then it can matter. However, again, it is the effect on strength drops that is the relevant aspect in this case as well. As an initial examination of fixed heterogeneities, we have considered multiplicative strength perturbations. As we have seen here, if the multiplicative perturbations are comparable to or larger than the strength drops, they can have a substantial effect on the resulting statistical behaviour of the population of events.

We have further seen that dynamic complexity persists even in the case of strong fixed heterogeneities, with no sign of periodic behaviour even at very large amplitudes of fixed multiplicative heterogeneities. At the same time, persistence of slip behaviours does increase with stronger heterogeneities for the large events, and the irregularity of large event repeat times decreases, although it does not disappear. For simple uniform fault attractors, heterogeneities increase the irregularity of large events. In both cases, most dramatically, spatial persistence of small events emerges with strong heterogeneities. This suggests persistence of the location of small events is a good signature of heterogeneity strength and is worth examining in earthquake data. Finally, from examining at finer scales the spatial structure of large event repeat time variance, we have seen a correlation of locations, with lower strength drop, having higher variation in large event repeat times; this may have important implications for more sophisticated estimates of earthquake hazard.

REFERENCES

Andrews, D.J. & Ben-Zion, Y., 1997. Wrinkle-like slip pulse on a fault between different materials, *J. geophys. Res.*, **102**, 553.

Ben-Zion, Y. & Rice, J.R., 1995. Slip patterns and earthquake populations along different classes of faults in elastic solids, *J. geophys. Res.*, **100**, 12 959.

Brune, J.N., 1996. Particle motions in a physical model of shallow angle thrust faulting, *Proc. Indian Acad. Sci. Earth planet. Sci.*, **105**, L197.

Carlson, J.M. & Langer, J.S., 1989. Mechanical model of an earthquake fault, *Phys. Rev. A*, **84**, 6470.

Carlson, J., Langer, J. & Shaw, B.E., 1994. Dynamics of earthquake faults, *Rev. Mod. Phys.*, **66**, 657.

Cochard, A. & Madariaga, R., 1996. Complexity of seismicity due to highly rate-dependent friction, *J. geophys. Res.*, **101**, 25 331.

Dieterich, J.H., 1979. Modeling of rock friction: 1 Experimental results and constitutive equations, *J. geophys. Res.*, **84**, 2161.

Ellsworth, W.L., Mathews, M.V., Nadeau, R.M., Nishenko, S.P., Reasenberg, P.A. & Simpson, R.W., 1999. A physically-based earthquake recurrence model for estimation of long-term earthquake probabilities, *USGS Open-File Report*, 99–522.

Fisher, D.S., Dahmen, K., Ramanathan, S. & Ben-Zion, Y., 1997. Statistics of earthquakes in simple models of heterogeneous faults, *Phys. Rev. Lett.*, **78**, 4885.

Knopoff, L., Landoni, J.A. & Abinante, M.S., 1992. Dynamic-model of an earthquake fault with localization, *Phys. Rev. A*, **46**, 7445.

Lamb, H., 1904. On the propagation of tremors over the surface of an elastic solid, *Philos. Trans. R. Soc. Lond. A*, **203**, 1.

Langer, J.S. & Nakanishi, H., 1993. Models of rupture propagation. II: Two dimensional model with dissipation on the fracture surface, *Phys. Rev. E*, **48**, 439.

Lin, B. & Taylor, P.L., 1994. Model of spatiotemporal dynamics of stick-slip motion, *Phys. Rev. E*, **49**, 3940.

Lindh, A.G., 2003. Long-term Earthquake forecasts in the San Francisco Bay Area: A contrarian perspective, *ESO Trans. AGU*, **84**, Fall Meet. Suppl., Abstract NG41C-0069.

Myers, C.H., Shaw, B.E. & Langer, J.S., 1996. Slip complexity in a crustal plane model of an earthquake fault, *Phys. Rev. Lett.*, **77**, 972.

Nielsen, S., Knopoff, L. & Tarantola, A., 1995. Model of earthquake recurrence: role of elastic wave radiation, relaxation of friction, and inhomogeneity, *J. geophys. Res.*, **100**, 12 423.

Nishenko, S.P. & Buland, R., 1987. A gereric recurrence interval distribution for earthquake forecasting, *Bull. seismol. Soc. Am.*, **77**, 1382.

Oglesby, D.D., Archuleta, R.J. & Nielsen, S.B., 1998. Earthquakes on dipping faults: the effects of broken symmetry, *J. geophys. Res.*, **280**, 1055.

Richards, P.G., 1979. Elementary solutions to Lamb's problem for a point source and their relevance to three dimensional studies of spontaneous crack propagation, *Bull. seism. Soc. Am.*, **69**, 947.

Ruina, A.L., 1983. Slip instability and state variable friction laws, *J. geophys. Res.*, **88**, 10 359.

Shaw, B.E., 1995. Frictional weakening and slip complexity on earthquake faults, *J. geophys. Res.*, **100**, 18 239.

Shaw, B.E., 1997. Modelquakes in the two dimensional wave equation, *J. geophys. Res.*, **102**, 27 367.

Shaw, B.E., 1998. Far field radiated energy scaling in elastodynamic earthquake fault models, *Bull. seism. Soc. Am.*, **88**, 1457.

Shaw, B.E., 2000. The edges of large earthquakes and the epicenters of future earthquakes: stress induced correlations in elastodynamic fault models, *Pure appl. Geophys.*, **157**, 2149.

Shaw, B.E., 2003. Magnitude dependence of radiated energy spectra: far field expressions of slip pulses in earthquake models, *J. geophys. Res.*, **108**, 2100, doi:10.1029/2001JB000741.

Shaw, B.E. & Rice, J.R., 2000. Existence of continuum complexity in the elastodynamics of repeated fault ruptures, *J. geophys. Res.*, **105**, 23 791.

Shaw, B.E. & Scholz, C.H., 2001. Slip-length scaling in large earthquakes: observations and theory and implications for earthquake physics, *Geophys. Res. Lett.*, **28**, 2995.

Sibson, R.H., 1973. Interactions between temperature and pore fluid pressure during earthquake faulting and a mechanism for partial or total stress relief, *Nature Phys. Sci.*, **243**, 66.

Wang, J.H. & Hwang, R.D., 2001. One-dimensional dynamic simulations of slip complexity of earthquake faults, *Earth Planets Space*, **53**, 91.

Weertman, J., 1980. Unstable slippage across a fault that separates elastic media of different elastic-constants, *J. geophys. Res.*, **85**, 1455.

Xu, H.J. & Knopoff, L., 1994. Periodicity and chaos in a one-dimensional dynamical model of earthquakes, *Phys. Rev. E*, **50**, 3577.